New Physics: Sae Mulli,
Vol. 75, No. 12, December 2025, pp. 944∼955
http://dx.doi.org/10.3938/NPSM.75.944

Quantum transport phenomena at oxide interfaces: Their potential for quantum science and technology

Yusuke KOZUKA*
Research Center for Materials Nanoarchitectonics (MANA),
National Institute for Materials Science (NIMS), Tsukuba 305-0047, Japan
Faculty of Science and Engineering, Waseda University, Tokyo 169-8555, Japan
WPI Advanced Institute for Materials Research, Tohoku University, Sendai 980-8577, Japan

(Received 16 October 2025 : revised 4 November 2025 : accepted 4 November 2025)

High-mobility charge carriers at semiconductor interfaces have provided fertile ground for the study of low-dimensional physics, such as the integer and fractional quantum Hall effects. In these studies, unique properties belonging to each material have not been explicitly highlighted, as the fundamental phenomena are believed to be universal and independent of the details of the materials. Here, we review high-mobility electrons at oxide interfaces, from fabrication to characterization. By incorporating the unique aspects of oxide materials as compared to conventional semiconductors, we can explore more diverse physics, including characteristic phenomena such as superconductivity and strong correlation. Finally, we discuss the prospects for potential quantum science and applications based on oxide interfaces.

Keywords: Oxides, Crystal growth, Quantum Hall effect, Superconductivity, Mesoscopic systems

I. INTRODUCTION

Conventionally, oxides were not regarded as promising platforms for condensed matter physics or major components of electronic devices because most of them are insulators. However, some researchers were drawn to the unique properties of conducting transition-metal oxides, which stem from the correlated nature of d electrons [1–3]. The situation changed dramatically with the discovery of high transition temperature (high-T_c) superconducting cuprates in 1986 [4, 5]. These materials promised unprecedented applications, such as superconducting magnets and superconducting quantum interference devices (SQUIDs) that operate above liquid nitrogen temperatures [6,7]. Furthermore, the high-T_c superconductivity and other related physical properties could not be easily explained within a single-particle picture, underscoring the need to explicitly consider electron correlations. Following this discovery, various oxide materials were investigated for both electronic applications and fundamental scientific research. This has led to the identification of many notable properties, including colossal magnetoresistance in manganites [8,9] and a large thermoelectric effect in cobaltites [10].

Despite many intriguing properties, one notably absent in oxides was high carrier mobility (μ), particularly in two dimensions, before the early 2000s. The electron correlation in transition-metal oxides might inherently limit high electron coherence due to the localizing nature of d electrons. However, the thin-film fabrication technologies for oxide materials were also underdeveloped, impeding the exploration of potentially high-mobility oxides. This situation stands in stark contrast to conventional semiconductors like GaAs, which exhibit extremely high electron mobility, even exceeding 10,000,000 cm^2/Vs below 4 K [11–13]. In the field of

*Correspondence to: KOZUKA.Yusuke@nims.go.jp

semiconductors, high-quality thin film and heterostructure fabrication technologies for certain materials underwent dramatic advancements in the 1980s and continue to progress even now. These advancements, coupled with sophisticated microfabrication techniques, have positioned GaAs as the dominant material for quantum devices such as quantum point contacts [14] and quantum dots [15].

In this review, we discuss advancements in high-mobility electron systems at oxide heterostructures. As mentioned above, many oxide materials face intrinsic challenges in achieving high carrier mobility due to strong electron correlation. However, there are notable exceptions, such as $SrTiO_3$ and ZnO. These materials have the potential to be utilized in various electronic and quantum devices, including field-effect transistors, quantum wires, and quantum dots, incorporating unique properties that are absent in conventional semiconductors. We also explore the future prospects of oxide-based quantum devices.

II. HIGH-MOBILITY ELECTRONS IN TWO DIMENSIONS

In this section, before reviewing oxide semiconductors, we explain the general background of the physics of high-mobility electrons in conventional semiconductors. High electron mobility, and consequently a long carrier scattering time (τ), is essential for observing quantum interference effects in solid-state materials. One typical quantum transport phenomenon is Shubnikov-de Haas (SdH) oscillations. In this phenomenon, circulating electrons form quantized energy levels under a strong magnetic field due to the interference of the wavefunction, resulting in resistance oscillations. The conditions to observe SdH oscillations are [16]

$$\hbar\omega_c \gg \hbar/\tau \ , \ k_B T \ ,$$

where $\hbar$ is the Planck constant (h) divided by 2π, ω_c ($= eB/m^*$, e: elementary charge of an electron, B: magnetic field, m^*: effective mass) is the cyclotron frequency, k_B is the Boltzmann constant, and T is the temperature. These conditions dictate that Landau level splitting energy ($\hbar\omega_c$) should be much larger than the energy broadening of the density of states due to carrier scattering ($\hbar/\tau$) and thermal broadening ($k_B T$). Assuming a relatively high magnetic field of 10 T, these conditions require parameters of $\mu \sim 10{,}000$ cm^2/Vs and $T \sim 1$ K.

While SdH oscillations have been utilized to obtain information about the Fermi surfaces in three-dimensional materials [17], more intriguing physics can be observed in two dimensions (2D) under a magnetic field due to well-defined integer filling numbers in the discrete Landau levels [18,19], known as the quantum Hall effect [20]. When the Fermi level is located in a mobility edge (localized states within a Landau level), all the electrons become localized due to circulating orbits [18,21], while an extended one-dimensional state remains along the edge of the sample [22]. This edge state carries charge current without dissipation because backscattering is completely prohibited due to the absence of the density of states of the counter-propagating channel. Simultaneously, opposing two edge states exhibit a constant difference in chemical potentials, resulting in a quantized Hall effect. The value of this effect is defined by the number of edge states (ν: filling factor) as $R_{yx} = h/\nu e^2 \approxeq 25.8\ \mathrm{k\Omega}/\nu$. Since the accuracy of the quantized Hall resistance is extremely precise, the quantum Hall effect is a promising candidate for resistance standards [23–25].

III. $SrTiO_3$

1. Basic properties

$SrTiO_3$ is known as a wide-gap semiconductor with a band gap of 3.2 eV [26]. Its most remarkable property is its high dielectric constant, which is approximately $\sim 300\varepsilon_0$ at room temperature and exceeds $20{,}000\varepsilon_0$ below 10 K (ε_0 is the vacuum permittivity) [27]. This large dielectric constant results from its incipient ferroelectric nature, which is suppressed by quantum fluctuations. When doped with Nb, La, or oxygen vacancies, $SrTiO_3$ becomes an n-type semiconductor. The electron mobility is typically around 10 cm^2/Vs at room temperature, but it dramatically increases to over 10,000 cm^2/Vs at low temperatures due to the large dielectric constant effectively screening impurity potentials [28–31]. This value

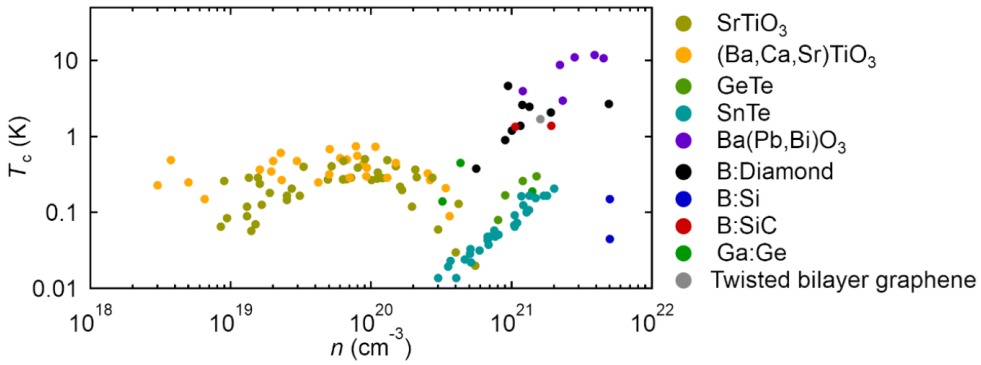

Fig. 1. (Color online) Superconducting temperature as a function of carrier density for various semiconductors. For twisted bilayer graphene, the thickness is roughly assumed to be 1 nm. Data are taken from Refs. [33–36] (n-$SrTiO_3$), [36,38] (n-(Ba,Ca,Sr)TiO_3), [39] (GeTe), [40] (SnTe), [41] (Ba(Pb,Bi)O_3), [42–44] (Diamond), [45] (B:Si), [46] (B:SiC), [47] (Ga:Ge), [48] (twisted bilayer graphene).

is extremely high compared to standard doped semiconductors, where impurity scattering becomes more dominant as the temperature decreases, following $\mu \propto T^{3/2}$ [32]. Moreover, doped $SrTiO_3$ exhibits superconductivity with a maximum superconducting temperature (T_c) of approximately 0.5 K at a carrier density of about 10^{20} cm^{-3} [33–36]. Although T_c itself is relatively low, this value is notably high when considering the density of states, as the Bardeen-Cooper-Schrieffer theory dictates that $k_B T_c \propto \exp(-1/NV)$, where N is the density of states at the Fermi energy and V is the coupling strength of a Cooper pair [37]. In fact, $SrTiO_3$ is among the superconductors with the lowest carrier densities known to date. For comparison, Fig. 1 shows several superconducting semiconductors with relatively low carrier densities [33–36,38–48].

2. Electron-doped $SrTiO_3$ thin film

Although bulk n-type $SrTiO_3$ exhibits high electron mobility, fabricating doped $SrTiO_3$ thin films with high electron mobility was challenging because the fabrication techniques for $SrTiO_3$ thin films were not well established until the early 2000s. At that time, the maximum electron mobility was limited to around 300 cm^2/Vs at low temperature [49, 50]. Instead, there were efforts to fabricate field-effect transistors (FETs) on bulk undoped $SrTiO_3$ to induce 2D electrons at the surface, similar to metal-oxide-semiconductor FETs in Si [51–53]. However, most efforts result in relatively low electron mobility less than 100 cm^2/Vs, due to damage to the $SrTiO_3$ surface during the deposition of insulators. To mitigate surface damage, FET structures using organic insulators or ionic liquids were developed, achieving mobilities of approximately 1,000 cm^2/Vs. However, SdH oscillations were not reported in these structures [54,55].

The challenge in growing bulk-quality $SrTiO_3$ thin films lies in controlling the Sr/Ti stoichiometry [56, 57]. High electron mobility is achieved below a carrier density of 10^{19} cm^{-3} [28–31], which corresponds to ~0.1 atomic % substitution of Nb in the Ti site. Even slight off-stoichiometry can cause carrier trapping at defects. One way to overcome this difficulty is to grow $SrTiO_3$ thin films at extremely high substrate temperatures, above ~1050 °C, where slight Sr/Ti off-stoichiometry can be solved by segregating a part of the off-stoichiometric components. Oxygen vacancies created during high-temperature growth can be filled by annealing in a moderate oxygen atmosphere of ~1 Pa, considering the defect formation properties of $SrTiO_3$ [58–61]. In fact, Nb-doped $SrTiO_3$ thin films grown at 1200 °C by pulsed laser deposition exhibit a high electron mobility of ~7,000 cm^2/Vs with 0.02 atomic % doping of Nb, which is close to the bulk value [62].

Another method involves using molecular beam epitaxy (MBE) with metal-organic gas sources for Ti, which enables the stoichiometric growth of La-doped $SrTiO_3$ thin films. In standard metal-source MBE, precise stoichiometric control is challenging unless one of the elements reevaporates to form a stoichiometric film. Both Sr and Ti metals have high melting temperatures, making

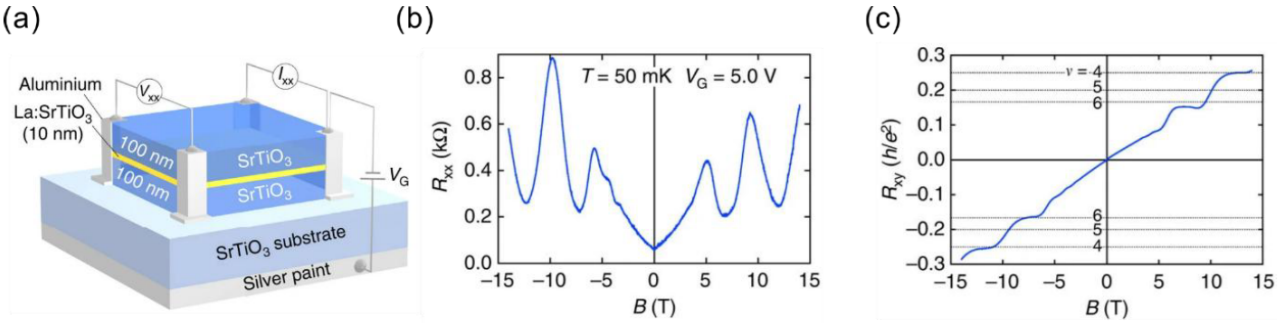

Fig. 2. (Color online) (a) Schematic diagram of the $SrTiO_3/n$-$SrTiO_3/SrTiO_3$ heterostructure. (b) Longitudinal resistance and (c) Hall resistance as a function of magnetic field of the heterostructure with a carrier density of 1.2×10^{12} cm^{-2}, measured at 50 mK. Adapted from Ref. [70].

reevaporation negligible at typical growth temperatures. However, using a metal-organic source allows for the self-organizing synthesis of stoichiometric $SrTiO_3$ thin films [63]. The maximum electron mobility of ∼0.001 atomic % La-doped $SrTiO_3$ shows an electron mobility of ∼30,000 cm^2/Vs [64].

3. 2D electron system in $SrTiO_3$

Conventionally, 2D electron systems in semiconductors are formed at the interface with a larger band gap material, such as in GaAs/(Al,Ga)As structures, where substituting Al with Ga widens the band gap and confines electrons within the GaAs layer [65]. However, band engineering is not well established in the case of $SrTiO_3$. Instead, homoepitaxial $SrTiO_3/n$-$SrTiO_3/SrTiO_3$ heterostructures, resembling δ-doped structures [66], are used to effectively confine electrons within the doped layer, where the n-$SrTiO_3$ layer is doped with either Nb or La [67,68]. When the n-$SrTiO_3$ layer is thin enough, below a typical de Broglie wavelength, the electron layer is regarded as 2D, and the angle dependence of SdH oscillations indicates a 2D Fermi surface [69]. However, the carrier density estimated from SdH oscillations is about one order of magnitude smaller than that estimated from the Hall effect. This discrepancy arises because the sheet carrier density cannot be reduced below $\sim 10^{13}$ cm^{-2} to maintain metallic conduction and, at this carrier density, multiple subbands are still partially filled. This issue was resolved by fabricating higher-quality heterostructures using metal-organic gas source MBE at high substrate temperatures, achieving a carrier density below 10^{12} cm^{-2} [70]. The quantum Hall effect was finally observed by modulating the carrier density using the $SrTiO_3$ substrate as a gate insulator as shown in Fig. 2 [70]. It is important to note that precise tuning of carrier density is essential, particularly considering the hysteretic gate dependence characteristic of the $SrTiO_3$ substrate as a gate insulator [71–73].

As with bulk-doped $SrTiO_3$, 2D electrons in $SrTiO_3$ heterostructures also exhibit superconductivity. By varying the thickness of the conducting layer, a 3D-2D crossover of superconductivity, as well as of electronic structures, were observed as shown in Fig. 3 [74]. Specifically, the dimensionality of superconductivity can be deduced from the temperature dependence of the upper critical field (B_{c2}) with magnetic fields applied in two different directions. When the magnetic field is perpendicular to the conducting plane, B_{c2} is expressed as

$$B_{c2}^{\perp}(T) = \frac{\phi_0}{2\pi\xi_{GL}(0)^2}\left(1 - \frac{T}{T_c}\right) ,$$

while for magnetic field parallel to the plane,

$$B_{c2}^{\parallel}(T) = \frac{\phi_0\sqrt{12}}{2\pi\xi_{GL}(0)d}\left(1 - \frac{T}{T_c}\right)^{1/2} ,$$

where ϕ_0 is the magnetic flux quantum, $\xi_{GL}(0)$ is the Ginzburg-Landau coherence length at low temperature, and d is the thickness of the superconducting layer. The second expression is valid for the two-dimensional superconductivity, where $d \ll \xi_{GL}$. These expressions of B_{c2} assume that Cooper pairs are broken by the vortex formation. In the $d \to 0$ limit, it becomes difficult for

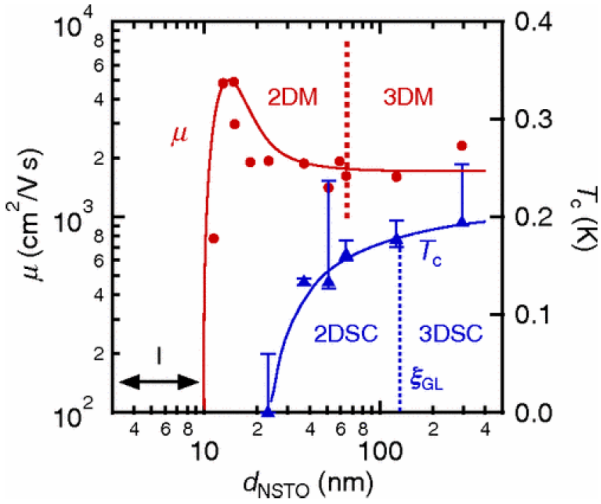

Fig. 3. (Color online) Electron mobility (μ) and superconducting transition temperature (T_c) as a function of doped layer thickness (d_{NSTO}) of the $SrTiO_3$/n-$SrTiO_3$/$SrTiO_3$ heterostructure. 3D-2D crossovers of electronic structure and superconductivity are also shown. I: insulator; 2DM: two-dimensional metal; 3DM: three-dimensional metal; 2DSC: two-dimensional superconductor; 3DSC: three-dimensional superconductor. Reprinted Fig. 5 with permission from [M. Kim *et al.*, Fermi surface and superconductivity in low-density high-mobility δ-doped $SrTiO_3$, Phys. Rev. Lett. **107**, 106801 (2011)] Copyright (2011) by the American Physical Society.

vortices to form under a parallel magnetic field. Instead, Zeeman energy breaks the pair potential of the Cooper pairs (Pauli paramagnetic limit), which is expressed as [75,76]

$$B_{c2}^{P} = \frac{\Delta_0}{\sqrt{2}\mu_B} = \frac{1.76 k_B T_c}{\sqrt{2}\mu_B} ,$$

where B_{c2}^{P} is the Pauli limiting field, Δ_0 is the superconducting gap energy in the weak-coupling limit, and μ_B is the Bohr magneton. The superconductivity of $SrTiO_3$ exceeds the Pauli paramagnetic limit by a factor of more than 4. This is believed to be due to spin-orbit interaction [77] as reported in the case of metal bilayer films [78]. The concept of breaking the Pauli paramagnetic limit through spin-orbit interaction has since been extended to other material systems, including transition-metal dichalcogenides [79,80].

4. Prospects for quantum devices of $SrTiO_3$

As mentioned above, doped $SrTiO_3$ is quite unique in that it exhibits superconductivity at very low carrier density. This property allows for superconductor-metal-insulator transitions to be controlled solely by electrostatic gating. By incorporating a split gate structure, superconducting weak links can be electrostatically formed as a foundation for quantum devices [81–83]. A similar device using other materials has only recently become possible with twisted bilayer graphene [84].

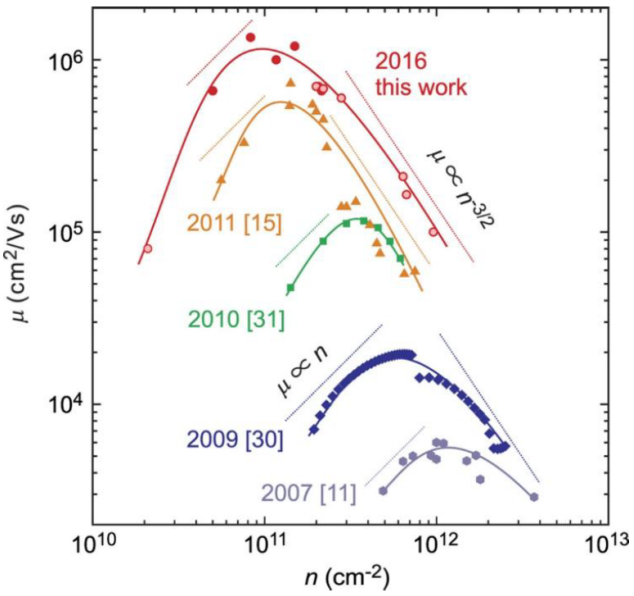

Fig. 4. (Color online) Advancements of electron mobility (μ) as a function of carrier density n for (Mg,Zn)O/ZnO heterostructures. Adapted from Ref. [106]. Reference numbers [11], [30], [31], and [15] in the figure correspond to Refs. [97], [103], [108], and [105] in this paper, respectively.

IV. ZnO

1. Crystal growth of ZnO thin films

ZnO is considered one of the typical II-VI semiconductors with a wide band gap of 3.37 eV. In terms of electronic applications, bulk ZnO has traditionally been used as a varistor [85]. However, until around the late 1990s, ZnO was not considered a promising material for electronic and quantum devices due to the immature growth techniques and the crystal quality, which was not comparable to that of other semiconductors. Below, the advancements in ZnO thin film growth are surveyed, as summarized in Fig. 4, in terms of electron mobility.

Research on ZnO thin films began to aim at applications such as transparent transistors [86, 87] or blue

and ultraviolet light-emitting diodes [88,89], leveraging its wide band gap. ZnO thin films were initially fabricated using pulsed laser deposition, and fundamental properties, including band gap modulation through Mg or Cd substitution, were investigated [90,91]. Mg and Cd are isovalent with Zn, and their substitution leads to structural changes and, consequently, band gap modifications, similar to Al or In substitution in GaAs. At the first stage, sapphire substrates were mostly used for growing ZnO thin films due to their commercial availability. However, the mobility of ZnO thin films was limited to around 100 cm^2/Vs due to the large lattice mismatch [92], which caused high-density dislocations. Later, more lattice-matched $ScAlMgO_4$ (SCAM) substrates were employed, leading to a maximum mobility of 5,000 cm^2/Vs, particularly when a high-temperature annealed Mg-substituted ZnO layer was used as a buffer layer [93]. The significant advancements in growth techniques, along with p-type doping using nitrogen, enabled the notable demonstration of a blue light-emitting diode [94,95].

Using the same growth technique and substrate, high-mobility 2D electrons were found to form at the ZnO/(Mg,Zn)O interface [96,97]. The accumulation of 2D electrons results from the relaxation of potential divergence, which is caused by the polarization discontinuity across the interface. ZnO has a Wurtzite crystal structure with inversion asymmetry, inherently possessing spontaneous polarization. The magnitude of this polarization varies with Mg substitution due to changes in the lattice constant and internal atomic coordinates. At the ZnO/(Mg,Zn)O interface, uncompensated charges are present, leading to the accumulation of 2D electrons [97,98]. Because of the high electron mobility, the quantum Hall effect was observed at low temperatures [97].

To further improve crystal quality and develop a method for mass production, two major advancements were made: the development of single-crystal ZnO substrates for homoepitaxy, and the use of molecular beam epitaxy (MBE). Single-crystal ZnO substrates were grown using the hydrothermal method [99]. The surface of the substrate was etched by diluted hydrochloric acid to prepare an epitaxy-ready surface [100]. In MBE, high-purity Zn and Mg metal sources were used along with oxygen plasma as the oxygen source. Compared to the single-crystal ZnO target used in pulsed laser deposition, the use of high-purity Zn and Mg metals significantly reduced the incorporation of impurities [101–103]. As a result, the electron mobility of the 2D electrons at the (Mg,Zn)O/ZnO interface increased to 100,000 cm^2/Vs [104]. Further improvements included optimizing the Mg content in the (Mg,Zn)O layer [105] and employing a pure ozone generator instead of oxygen plasma for the oxygen source [106]. Notably, using pure ozone expanded the growth temperature window to lower temperatures, from ∼900 °C with oxygen plasma to ∼750 °C, reducing the incorporation of impurities from surrounding components of the substrate. These efforts led to a record mobility of over 1,000,000 cm^2/Vs [107].

2. Quantum Hall effect in ZnO

As mentioned above, the integer quantum Hall effect was first observed in ZnO heterostructures with an electron mobility of ∼5,000 cm^2/Vs, fabricated using pulsed laser deposition [97]. By employing MBE, the electron mobility increased to 100,000 cm^2/Vs, leading to the observation of the fractional quantum Hall effect [108,109]. In this phenomenon, electron correlation plays an essential role in forming fractionally charged quasiparticles known as composite fermions.

Although the quantum Hall effect is a universal phenomenon regardless of the material, the specifics of the integer and fractional quantum Hall effects significantly depend on various factors, such as the strength of electron correlations. The strength of the correlation for itinerant electrons is expressed based on the ratio of the Coulomb energy to the kinetic energy as

$$r_{\mathrm{s}} = \frac{m^* e^2}{4\pi\varepsilon\hbar^2\sqrt{n\pi}} ,$$

where ε is the dielectric constant and n is the sheet carrier density. As shown in Fig. 5 [11–13,106,109–120], r_{s} parameter of ZnO is significantly larger than that of other typical high-mobility 2D systems while maintaining high scattering time. One notable consequence of this is the enhancement of electron susceptibility, which is the product of the effective g-factor and the effective mass [121,122]. The electron susceptibility was experimentally

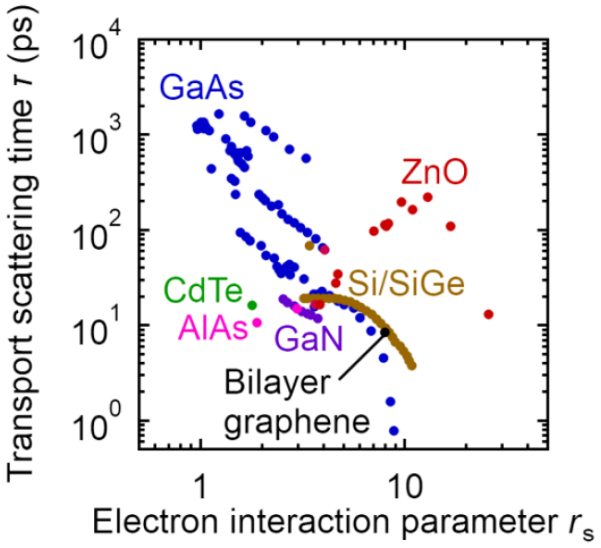

Fig. 5. (Color online) Mapping of transport scattering time (τ) and electron interaction parameter (r_s) for several high-mobility 2D carriers. Data are taken from Refs. [11–13,110–112] (GaAs), [113,114] (Si/SiGe), [115] (CdTe), [116–118] (AlAs), [119] (GaN), [120] (bilayer graphene), and [106] (ZnO).

estimated using the coincidence method, where the cyclotron energy is an integer multiple of the Zeeman energy, leading to a double period of SdH oscillations as a function of $1/B$.

Another notable finding is the even-denominator fractional quantum Hall effect [123]. Usually, the filling factor has an odd denominator to comply with the Pauli exclusion principle [124, 125]. However, when composite fermions form pairs due to effective attraction, the fractional quantum Hall effect with an even denominator filling can be observed [126]. This phenomenon has been observed in extremely high-quality GaAs heterostructures. ZnO has become another example exhibiting the even-denominator fractional quantum Hall effect [127,128]. Notably, ZnO shows a greater variety of even-denominator fractional quantum Hall effects by rotating the conducting plane with respect to the magnetic field, including $\nu = 3/2$, $5/2$ and $7/2$. In contrast, GaAs mostly shows $\nu = 5/2$ and, in very rare cases, $\nu = 7/2$ [129], but the signal easily diminishes with increasing in-plane magnetic field [130]. This variety of fractional states in ZnO is attributed to the strong electron correlation and the resulting complex energy diagram, which originates from large and nonlinear electron susceptibility [131].

3. Prospects for quantum devices

A high-quality 2D electron system is essential for constructing more complex quantum devices, such as quantum point contacts or quantum dots. ZnO, in particular, possesses promising properties for the application of spin qubits. Firstly, only 2% of natural Zn isotopes (^{67}Zn) include nuclear spins, which minimizes the loss of spin information [132]. Secondly, ZnO is a direct band gap semiconductor, and its conduction band consists of a single electron pocket, thus eliminating interband scattering, unlike in Si. These two factors combine the advantageous aspects of both GaAs (single electron pocket) and Si (low-density nuclear spins). The spin coherence time of ZnO has been theoretically predicted to be relatively long [133], even compared with Si and diamond, which are under intensive study for quantum sensing applications. Experimentally, a long longitudinal spin coherence time (T_1) of ~500 ms has been observed for electrons bound around Al donors [134,135]. Additionally, electrostatically defined quantum dots have been demonstrated, marking an important step toward realizing spin qubits using ZnO heterostructures [136]. The unique properties of ZnO, combined with these experimental advancements, are expected to lead to superior functionalities in quantum devices.

ACKNOWLEDGEMENTS

The author thanks all the collaborators and particularly acknowledges C. Bell, J. Falson, Y. Hikita, H. Y. Hwang, M. Kawasaki, M. Kim, D. Maryenko, and A. Tsukazaki. This work is partly supported by JST FOREST Program (Grant Number: JPMJFR203D) and by JSPS KAKENHI (23K26482, 25H00613). MANA and AIMR are supported by World Premier International Research Center Initiative (WPI), MEXT, Japan.

REFERENCES

[1] C. N. R. Rao and G. V. S. Rao, Electrical conduction in metal oxides, Phys. Stat. Sol. (a) **1**, 597 (1970).

[2] J. B. Goodenough, Metallic oxides, Prog. Solid State Chem. **5**, 145 (1971).

[3] J. B. Torrance, P. Lacorre, C. Asavaroengchai and R. M. Metzger, Why are some oxides metallic, while most are insulating?, Physica C **182**, 351 (1991).

[4] J. G. Bednorz and K. A. Müller, Possible high T_c superconductivity in the Ba-La-Cu-O system, Z. Phys. B **64**, 189 (1986).

[5] J. G. Bednorz and K. A. Müller, Perovskite-type oxides-The new approach to high-T_c superconductivity, Rev. Mod. Phys. **60**, 585 (1988).

[6] D. Uglietti, A review of commercial high temperature superconducting materials for large magnets: From wires and tapes to cables and conductors, Supercond. Sci. Technol. **32**, 053001 (2019).

[7] D. Koelle *et al.*, High-transition-temperature superconducting quantum interference devices, Rev. Mod. Phys. **71**, 631 (1999).

[8] S. Jin *et al.*, Thousandfold change in resistivity in magnetoresistive La-Ca-Mn-O films, Science **264**, 413 (1994).

[9] Y. Tokura, Critical features of colossal magnetoresistive manganites, Rep. Prog. Phys. **69**, 797 (2006).

[10] I. Terasaki, Y. Sasago and K. Uchinokura, Large thermoelectric power in $NaCo_2O_4$ single crystals, Phys. Rev. B **56**, R12685 (1997).

[11] L. Pfeiffer and K. W. West, The role of MBE in recent quantum Hall effect physics discoveries, Physica E **20**, 57 (2003).

[12] V. Umansky *et al.*, MBE growth of ultra-low disorder 2DEG with mobility exceeding 35×10^6 cm^2/Vs, J. Cryst. Growth **311**, 1658 (2009).

[13] Y. J. Chung *et al.*, Ultra-high-quality two-dimensional electron systems, Nat. Mater. **20**, 632 (2021).

[14] H. van Houten, C. W. Beenakker and B. J. van Wees, in *Semiconductors and Semimetals: Nanostructured Systems*, edited by M. Reed (Academic, New York, 1992), Vol. 35, p. 9.

[15] L. P. Kouwenhoven, D. G. Austing and S. Tarucha, Few-electron quantum dots, Rep. Prog. Phys. **64**, 701 (2001).

[16] L. M. Roth and P. N. Argyres, in *Semiconductors and Semimetals: Physics of III-V Compounds*, edited by R. K. Willardson and A. C. Beer (Academic, New York, 1966), Vol. 1, Chap. 6.

[17] N. Ashcroft and N. D. Mermin, *Solid State Physics* (Saunders College Publishing, Philadelphia, 1976).

[18] D. Yoshioka, *The Quantum Hall Effect* (Springer, Heidelberg, 2002).

[19] M. Kohmoto, Topological invariant and the quantization of the Hall conductance, Ann. Phys. **160**, 343 (1985).

[20] K. v. Klitzing, G. Dorda and M. Pepper, New method for high-accuracy determination of the fine-structure constant based on quantized Hall resistance, Phys. Rev. Lett. **45**, 494 (1980).

[21] K. v. Klitzing, The quantized hall effect, Physica B+C **126**, 242 (1984).

[22] R. J. Haug, Edge-state transport and its experimental consequences in high magnetic fields, Semicond. Sci. Technol. **8**, 131 (1993).

[23] A. Hartland, The quantum Hall effect and resistance standards, Metrologia **29**, 175 (1992).

[24] B. Jeckelmann and B. Jeanneret, The quantum Hall effect as an electrical resistance standard, Rep. Prog. Phys. **64**, 1603 (2001).

[25] K. v. Klitzing, Essay: Quantum Hall effect and the new international system of units, Phys. Rev. Lett. **122**, 200001 (2019).

[26] J. A. Noland, Optical absorption of single-crystal strontium titanate, Phys. Rev. **94**, 724 (1954).

[27] K. A. Müller and H. Burkard, $SrTiO_3$: An intrinsic quantum paraelectric below 4 K, Phys. Rev. B **19**, 3593 (1979).

[28] J. F. Schooley, W. R. Hosler and M. L. Cohen, Superconductivity in semiconducting $SrTiO_3$, Phys. Rev. Lett. **12**, 474 (1964).

[29] O. N. Tufte and P. W. Chapman, Electron mobility in semiconducting strontium titanate, Phys. Rev. **155**, 796 (1967).

[30] H. P. R. Frederikse and W. R. Hosler, Hall mobility in $SrTiO_3$, Phys. Rev. **161**, 822 (1967).

[31] G. Perluzzo and J. Destry, The characterization of pure and niobium-doped crystals of strontium titanate using Hall, electrical conductivity, and optical absorption data, Can. J. Phys. **56**, 453 (1978).

[32] P. Y. Yu and M. Cardona, *Fundamentals of Semiconductors: Physics and Materials Properties* (Springer, Heidelberg, 1996).

[33] C. S. Koonce *et al.*, Superconducting transition temperatures of semiconducting $SrTiO_3$, Phys. Rev. **163**, 380 (1967).

[34] H. Suzuki *et al.*, Superconductivity in single-crystalline $Sr_{1-x}La_xTiO_3$, J. Phys. Soc. Jpn. **65**, 1529 (1996).

[35] Y. Tomioka, N. Shirakawa, K. Shibuya and I. H. Inoue, Enhanced superconductivity close to a non-magnetic quantum critical point in electron-doped strontium titanate, Nat. Commun. **10**, 738 (2019).

[36] Y. Tomioka, N. Shirakawa and I. H. Inoue, Superconductivity enhancement in polar metal regions of $Sr_{0.95}Ba_{0.05}TiO_3$ and $Sr_{0.985}Ca_{0.015}TiO_3$ revealed by systematic Nb doping, npj Quantum Mater. **7**, 111 (2022).

[37] M. Tinkham, *Introduction to Superconductivity*, 2nd ed. (McGraw-Hill Inc., Singapore, 2004).

[38] J. F. Schooley, H. P. R. Frederikse, W. R. Hosler and E. R. Pfeiffer, Superconductive properties of ceramic mixed titanates, Phys. Rev. **159**, 301 (1967).

[39] R. A. Hein *et al.*, Superconductivity in germanium telluride, Phys. Rev. Lett. **12**, 320 (1964).

[40] J. K. Hulm *et al.*, Superconducting interactions in tin telluride, Phys. Rev. **169**, 388 (1968).

[41] T. D. Thanh, A. Koma and S. Tanaka, Superconductivity in the $BaPb_{1-x}Bi_xO_3$ system, Appl. Phys. **22**, 205 (1980).

[42] E. A. Ekimov *et al.*, Superconductivity in diamond, Nature **428**, 542 (2004).

[43] E. Bustarret *et al.*, Dependence of the superconducting transition temperature on the doping level in single-crystalline diamond films, Phys. Rev. Lett. **93**, 237005 (2004).

[44] K. Winzer, D. Bogdanov and Ch. Wild, Electronic properties of boron-doped diamond on the border between the normal and the superconducting state, Physica C **432**, 65 (2005).

[45] E. Bustarret *et al.*, Superconductivity in doped cubic silicon, Nature **444**, 465 (2006).

[46] Z.-A. Ren *et al.*, Superconductivity in Boron-doped SiC, J. Phys. Soc. Jpn. **76**, 103710 (2007).

[47] T. Hermannsdörfer *et al.*, Superconducting state in a gallium-doped germanium layer at low temperatures, Phys. Rev. Lett. **102**, 217003 (2009).

[48] Y. Cao *et al.*, Unconventional superconductivity in magic-angle graphene superlattices, Nature **556**, 43 (2018).

[49] A. Leitner *et al.*, Pulsed laser deposition of superconducting Nb-doped strontium titanate thin films, Appl. Phys. Lett. **72**, 3065 (1998).

[50] D. Olaya, F. Pan, C. T. Rogers and J. C. Price, Electrical properties of La-doped strontium titanate thin films, Appl. Phys. Lett. **80**, 2928 (2002).

[51] K. Ueno *et al.*, Field-effect transistor on $SrTiO_3$ with sputtered Al_2O_3 gate insulator, Appl. Phys. Lett. **83**, 1755 (2003).

[52] K. Shibuya *et al.*, Single crystal $SrTiO_3$ field-effect transistor with an atomically flat amorphous $CaHfO_3$ gate insulator, Appl. Phys. Lett. **85**, 425 (2004).

[53] K. Shibuya, T. Ohnishi, T. Sato and M. Lippmaa, Metal-insulator transition in $SrTiO_3$ induced by field effect, J. Appl. Phys. **102**, 083713 (2007).

[54] H. Nakamura *et al.*, Low temperature metallic state induced by electrostatic carrier doping of $SrTiO_3$, Appl. Phys. Lett. **89**, 133504 (2006).

[55] K. Ueno *et al.*, Electric-field-induced superconductivity in an insulator, Nat. Mater. **7**, 855 (2008).

[56] T. Ohnishi *et al.*, Improved stoichiometry and misfit control in perovskite thin film formation at a critical fluence by pulsed laser deposition, Appl. Phys. Lett. **87**, 241919 (2005).

[57] T. Ohnishi, K. Shibuya, T. Yamamoto and M. Lippmaa, Defects and transport in complex oxide thin films, J. Appl. Phys. **103**, 103703 (2008).

[58] G. Horvath, J. Gerblinger, H. Meixner and J. Giber, Segregation driving forces in perovskite titanates, Sens. Actuator B: Chem. **32**, 93 (1996).

[59] R. Moos and K. H. Härdtl, Defect chemistry of donor-doped and undoped strontium titanate ceramics between 1000° and 1400 °C, J. Am. Ceram. Soc. **80**, 2549 (1997).

[60] K. Szot and W. Speier, Surfaces of reduced and oxidized $SrTiO_3$ from atomic force microscopy, Phys. Rev. B **60**, 5909 (1999).

[61] R. Meyer, R. Waser, J. Helmbold and G. Borchardt, Cationic surface segregation in donor-doped $SrTiO_3$ under oxidizing conditions, J. Electroceram. **9**, 101 (2002).

[62] Y. Kozuka, Y. Hikita, C. Bell and H. Y. Hwang, Dramatic mobility enhancements in doped $SrTiO_3$ thin films by defect management, Appl. Phys. Lett. **97**, 012107 (2010).

[63] B. Jalan, P. Moetakef and S. Stemmer, Molecular beam epitaxy of $SrTiO_3$ with a growth window, Appl. Phys. Lett. **95**, 032906 (2009).

[64] J. Son *et al.*, Epitaxial $SrTiO_3$ films with electron mobilities exceeding 30,000 $cm^2V^{-1}s^{-1}$, Nat. Mater. **9**, 482 (2010).

[65] R. Dingle, H. L. Stömer, A. C. Gossard and W. Wiegmann, Electron mobilities in modulation-doped semiconductor heterojunction superlattices, Appl. Phys. Lett. **33**, 665 (1978).

[66] E. F. Schubert and K. Ploog, The δ-Doped field-effect transistor, Jpn. J. Appl. Phys. **24**, L608 (1985).

[67] Y. Kozuka *et al.*, Enhancing the electron mobility via delta-doping in $SrTiO_3$, Appl. Phys. Lett. **97**, 222115 (2010).

[68] B. Jalan, S. Stemmer, S. Mack and S. J. Allen, Two-dimensional electron gas in δ-doped $SrTiO_3$, Phys. Rev. B **82**, 081103(R) (2010).

[69] Y. Kozuka *et al.*, Two-dimensional normal-state quantum oscillations in a superconducting heterostructure, Nature **462**, 487 (2009).

[70] Y. Matsubara *et al.*, Observation of the quantum Hall effect in δ-doped $SrTiO_3$, Nat. Commun. **7**, 11631 (2016).

[71] J. Biscaras *et al.*, Limit of the electrostatic doping in two-dimensional electron gases of $LaXO_3$(X = Al, Ti)/$SrTiO_3$, Sci. Rep. **4**, 6788 (2014).

[72] W. Liu *et al.*, Magneto-transport study of top- and back-gated $LaAlO_3/SrTiO_3$ heterostructures, APL Mater. **3**, 062805 (2015).

[73] C. Yin *et al.*, Electron trapping mechanism in $LaAlO_3/SrTiO_3$ heterostructures, Phys. Rev. Lett. **124**, 017702 (2020).

[74] M. Kim *et al.*, Fermi surface and superconductivity in low-density high-mobility δ-doped $SrTiO_3$, Phys. Rev. Lett. **107**, 106801 (2011).

[75] B. S. Chandrasekhar, A note on the maximum critical field of high-field superconductors, Appl. Phys. Lett. **1**, 7 (1962).

[76] A. M. Clogston, Upper limit for the critical field in hard superconductors, Phys. Rev. Lett. **9**, 266 (1962).

[77] M. Kim *et al.*, Intrinsic spin-orbit coupling in superconducting δ-doped $SrTiO_3$ heterostructures, Phys. Rev. B **86**, 085121 (2012).

[78] X. S. Wu, P. W. Adams, Y. Yang and R. L. McCarley, Spin proximity effect in ultrathin superconducting Be-Au bilayers, Phys. Rev. Lett. **96**, 127002 (2006).

[79] Y. Saito *et al.*, Superconductivity protected by spin–valley locking in ion-gated MoS_2, Nat. Phys. **12**, 144 (2016).

[80] J. M. Lu *et al.*, Evidence for two-dimensional Ising superconductivity in gated MoS_2, Science **350**, 1353 (2015).

[81] P. Gallagher, M. Lee, J. R. Williams and D. Goldhaber-Gordon, Gate-tunable superconducting weak link and quantum point contact spectroscopy on a strontium titanate surface, Nat. Phys. **10**, 748 (2014).

[82] H. Thierschmann *et al.*, Transport regimes of a split gate superconducting quantum point contact in the two-dimensional $LaAlO_3/SrTiO_3$ superfluid, Nat. Commun. **9**, 2276 (2018).

[83] E. Mikheev, I. T. Rosen and D. Goldhaber-Gordon, Quantized critical supercurrent in $SrTiO_3$-based quantum point contacts, Sci. Adv. **7**, eabi6520 (2021).

[84] E. Portolés *et al.*, A tunable monolithic SQUID in twisted bilayer graphene, Nat. Nanotechnol. **17**, 1159 (2022).

[85] D. R. Clarke, Varistor ceramics, J. Am. Ceram. Soc. **82**, 485 (1999).

[86] J. Nishii *et al.*, High mobility thin film transistors with transparent ZnO channels, Jpn. J. Appl. Phys. **42**, L347 (2003).

[87] T. Minami, Transparent conducting oxide semiconductors for transparent electrodes, Semicond. Sci. Technol. **20**, S35 (2005).

[88] Z. K. Tnag *et al.*, Room-temperature ultraviolet laser emission from self-assembled ZnO microcrystallite thin films, Appl. Phys. Lett. **72**, 3270 (1998).

[89] M. Kawasaki *et al.*, Excitonic ultraviolet laser emission at room temperature from naturally made cavity in ZnO nanocrytal thin films, Mater. Sci. Eng. B **56**, 239 (1998).

[90] A. Ohtomo *et al.*, $Mg_xZn_{1-x}O$ as a II–VI widegap semiconductor alloy, Appl. Phys. Lett. **72**, 2466 (1998).

[91] T. Makino *et al.*, Band gap engineering based on $Mg_xZn_{1-x}O$ and $Cd_yZn_{1-y}O$ ternary alloy films, Appl. Phys. Lett. **78**, 1237 (2001).

[92] A. Ohtomo *et al.*, Single crystalline ZnO films grown on lattice-matched $ScAlMgO_4$ (0001) substrates, Appl. Phys. Lett. **75**, 2635 (1999).

[93] A. Tsukazaki, A. Ohtomo and M. Kawasaki, High-mobility electronic transport in ZnO thin films, Appl. Phys. Lett. **88**, 152106 (2006).

[94] A. Tsukazaki *et al.*, Repeated temperature modulation epitaxy for p-type doping and light-emitting diode based on ZnO, Nat. Mater. **4**, 42 (2005).

[95] A. Tsukazaki *et al.*, Blue light-emitting diode based on ZnO, Jpn. J. Appl. Phys. **44**, L643 (2005).

[96] H. Tampo *et al.*, Two-dimensional electron gas in Zn polar ZnMgO/ZnO heterostructures grown by radical source molecular beam epitaxy, Appl. Phys. Lett. **89**, 132113 (2006).

[97] A. Tsukazaki *et al.*, Quantum Hall effect in polar oxide heterostructures, Science **315**, 1388 (2007).

[98] A. Malashevich and D. Vanderbilt, First-principles study of polarization in $Zn_{1-x}Mg_xO$, Phys. Rev. B **75**, 045106 (2007).

[99] K. Maeda, M. Sato, I. Niikura and T. Fukuda, Growth of 2 inch ZnO bulk single crystal by the hydrothermal method, Semicond. Sci. Technol. **20**, S49 (2005).

[100] S. Akasaka *et al.*, Preparation of an epitaxy-ready surface of a ZnO(0001) substrate, Appl. Phys. Express **4**, 035701 (2011).

[101] A. Tsukazaki *et al.*, High electron mobility exceeding 10^4 cm^2 V^{-1}s^{-1} in $Mg_xZn_{1-x}O$/ZnO single heterostructures grown by molecular beam epitaxy, Appl. Phys. Express **1**, 055004 (2008).

[102] S. Akasaka *et al.*, $Mg_xZn_{1-x}O$ films with a low residual donor concentration ($<10^{15}$ cm^{-3}) grown by molecular beam epitaxy, Appl. Phys. Express **3**, 071101 (2010).

[103] M. Nakano *et al.*, Electronic-field control of two-dimensional electrons in polymer-gated–oxide semiconductor heterostructures, Adv. Mater. **22**, 876 (2010).

[104] S. Akasaka *et al.*, Improvement of electron mobility above 100,000 cm^2 V^{-1}s^{-1} in $Mg_xZn_{1-x}O$/ZnO heterostructures, Jpn. J. Appl. Phys. **50**, 080215 (2011).

[105] J. Falson *et al.*, Magnesium doping controlled density and mobility of two-dimensional electron gas in $Mg_xZn_{1-x}O$/ZnO heterostructures, Appl. Phys. Express **4**, 091101 (2011).

[106] J. Falson *et al.*, MgZnO/ZnO heterostructures with electron mobility exceeding 1×10^6 cm^2/Vs, Sci. Rep. **6**, 26598 (2016).

[107] J. Falson *et al.*, Electron scattering times in ZnO based polar heterostructures, Appl. Phys. Lett. **107**, 082102 (2015).

[108] A. Tsukazaki *et al.*, Observation of the fractional quantum Hall effect in an oxide, Nat. Mater. **9**, 889 (2010).

[109] Y. Kozuka *et al.*, Insulating phase of a two-dimensional electron gas in $Mg_xZn_{1-x}O$/ZnO heterostructures below $\nu = 1/3$, Phys. Rev. B **84**, 033304 (2011).

[110] L. N. Pfeiffer, K. W. West, H. L. Stormer and K. W. Baldwin, Electron mobilities exceeding 10^7 cm^2/Vs in modulation-doped GaAs, Appl. Phys. Lett. **55**, 1888 (1989).

[111] T. Sajoto *et al.*, Fractional quantum Hall effect in very-low-density $GaAs/Al_xGa_{1-x}As$ heterostructures, Phys. Rev. B **41**, 8449 (1990).

[112] G. C. Gardner, S. Fallahi, J. D. Watson and M. J. Manfra, Modified MBE hardware and techniques and role of gallium purity for attainment of two dimensional electron gas mobility $>35\times10^6$ cm^2/Vs in AlGaAs/GaAs quantum wells grown by MBE, J. Cryst. Growth **441**, 71 (2016).

[113] T. M. Lu, D. C. Tsui, C.-H. Lee and C. W. Liu, Observation of two-dimensional electron gas in a Si quantum well with mobility of 1.6×10^6 cm^2/Vs, Appl. Phys. Lett. **94**, 182102 (2009).

[114] T. M. Lu *et al.*, Fractional quantum Hall effect of two-dimensional electrons in high-mobility Si/SiGe field-effect transistors, Phys. Rev. B **85**, 121307(R) (2012).

[115] B. A. Piot *et al.*, Fractional quantum Hall effect in CdTe, Phys. Rev. B **82**, 081307(R) (2010).

[116] E. P. De Poortere *et al.*, Enhanced electron mobility and high order fractional quantum Hall states in AlAs quantum wells, Appl. Phys. Lett. **80**, 1583 (2002).

[117] A. V. Shchepetilnikov *et al.*, $\nu = 2/3$ fractional quantum Hall state in an AlAs quantum well probed by electron spin resonance, Phys. Rev. B **96**, 161301(R) (2017).

[118] Md. S. Hossain *et al.*, Valley-tunable even-denominator fractional quantum Hall state in the lowest Landau level of an anisotropic system, Phys. Rev. Lett. **130**, 126301 (2023).

[119] M. J. Manfra *et al.*, Electron mobility exceeding 160000 cm^2/Vs in AlGaN/GaN heterostructures grown by molecular-beam epitaxy, Appl. Phys. Lett. **85**, 5394 (2004).

[120] T. Iwasaki *et al.*, Bubble-free transfer technique for high-quality graphene/hexagonal boron nitride van der Waals heterostructures, ACS Appl. Mater. Interfaces **12**, 8533 (2020).

[121] Y. Kozuka *et al.*, Single-valley quantum Hall ferromagnet in a dilute $Mg_xZn_{1-x}O$/ZnO strongly correlated two-dimensional electron system, Phys. Rev. B **85**, 075302 (2012).

[122] D. Maryenko *et al.*, Temperature-dependent magnetotransport around $\nu = 1/2$ in ZnO heterostructures, Phys. Rev. Lett. **108**, 186803 (2012).

[123] R. Willett *et al.*, Observation of an even-denominator quantum number in the fractional quantum Hall effect, Phys. Rev. Lett. **59**, 1776 (1987).

[124] D. C. Tsui, H. L. Stormer and A. C. Gossard, Two-dimensional magnetotransport in the extreme quantum limit, Phys. Rev. Lett. **48**, 1559 (1982).

[125] R. B. Laughlin, Anomalous quantum Hall effect: An incompressible quantum fluid with fractionally charged excitations, Phys. Rev. Lett. **50**, 1395 (1983).

[126] V. W. Scarola, K. Park and J. K. Jain, Cooper instability of composite fermions, Nature **406**, 863 (2000).

[127] J. Falson *et al.*, Even-denominator fractional quantum Hall physics in ZnO, Nat. Phys. **11**, 347 (2015).

[128] J. Falson *et al.*, A cascade of phase transitions in an orbitally mixed half-filled Landau level, Sci. Adv. **4**, eaat8742 (2018).

[129] J. Shabani, Y. Lin and M. Shayegan, Fractional quantum Hall effect at high fillings in a two-subband electron system, Phys. Rev. Lett. **105**, 246805 (2010).

[130] C. R. Dean *et al.*, Contrasting behavior of the 5/2 and 7/3 fractional quantum Hall effect in a tilted field, Phys. Rev. Lett. **101**, 186806 (2008).

[131] D. Maryenko *et al.*, Polarization-dependent Landau level crossing in a two-dimensional electron system in a MgZnO/ZnO heterostructure, Phys. Rev. B **90**, 245303 (2014).

[132] I. A. Merkulov, A. L. Efros and M. Rosen, Electron spin relaxation by nuclei in semiconductor quantum dots, Phys. Rev. B **65**, 205309 (2002).

[133] S. Kanai *et al.*, Generalized scaling of spin qubit coherence in over 12,000 host materials, Proc. Acad. Nat. Sci. **119**, e2121808119 (2022).

[134] X. Linpeng *et al.*, Coherence properties of shallow donor qubits in ZnO, Phys. Rev. Appl. **10**, 064061 (2018).

[135] V. Niaouris *et al.*, Ensemble spin relaxation of shallow donor qubits in ZnO, Phys. Rev. B **105**, 195202 (2022).

[136] K. Noro *et al.*, Parity-independent Kondo effect of correlated electrons in electrostatically defined ZnO quantum dots, Nat. Commun. **15**, 9556 (2024).